HHS Public Access

Author manuscript

Chem Commun (Camb). Author manuscript; available in PMC 2019 May 03.

Published in final edited form as:

Chem Commun (Camb). 2018 May 03; 54(37): 4681–4684. doi:10.1039/c8cc01297k.

A Photoactive Semisynthetic Metalloenzyme Exhibits Complete Selectivity for CO_2 Reduction in Water

Camille R. Schneider[a], **Anastasia C. Manesis**[a], **Michael J. Stevenson**[b,†], and **Hannah S. Shafaat**[a,b]

[a]Ohio State Biochemistry Program, The Ohio State University, Columbus, OH 43210 USA; Phone: +1-614-688-1982

[b]Department of Chemistry and Biochemistry, The Ohio State University, Columbus, OH 43210 USA

Abstract

A series of artificial metalloenzymes containing a ruthenium chromophore and $[Ni^{II}(cyclam)]^{2+}$, both incorporated site-selectively, have been constructed within an azurin protein scaffold. These light-driven, semisynthetic enzymes do not evolve hydrogen, thus displaying complete selectivity for CO_2 reduction to CO. Electrostatic effects rather than direct excited-state electron transfer dominate the ruthenium photophysics, suggesting that intramolecular electron transfer from photogenerated Ru^{I} to $[Ni^{II}(cyclam)]^{2+}$ represents the first step in catalysis. Stern-Volmer analyses rationalize the observation that ascorbate is the only sacrificial electron donor that supports turnover. Collectively, these results highlight the important interplay of elements that must be considered when developing and characterizing molecular catalysts.

Graphical abstract

An artificial metalloenzyme reduces CO2 to CO using light, suggesting intramolecular electron transfer and secondary sphere effects modulate catalytic selectivity.

Correspondence to: Hannah S. Shafaat.

†Current address: Department of Chemistry and Biochemistry, University of California at Davis, Davis, CA 95616 USA

Electronic Supplementary Information (ESI) available: Detailed materials and methods, MALDI-TOF M/S, UV-Vis, luminescence and TCSPC traces, and control GC experiments.

There are no conflicts of interest to declare.

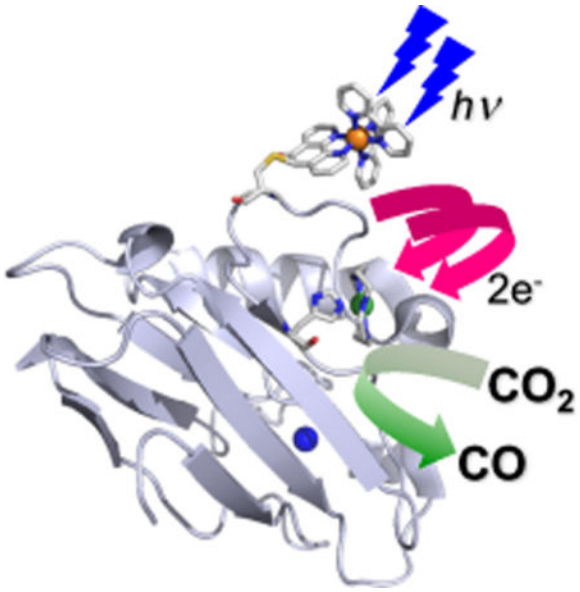

The continued rise in atmospheric carbon dioxide levels has resulted in renewed focus on developing efficient catalysts for CO_2 conversion into chemical feedstocks.[1–3] Of these, the two-electron reduction of CO_2 to carbon monoxide (CO) is of particular interest for use in downstream industrial applications. While performing these reactions in aqueous media would be environmentally benign, selectivity remains a primary challenge for this field owing to similar thermodynamic potentials for proton reduction to hydrogen and CO_2 conversion into C_1 products.[4] A variety of approaches spanning biological, synthetic, and materials science fields have been employed to tackle this problem.[5–9] Recently, engineering proteins has emerged as a viable strategy to combine specific advantages of many of these approaches, including manipulation of defined primary and secondary coordination spheres, natural cofactor substitution,[10,11] water solubility, and construction of tailored interfaces.[12–17]

We have elected to employ a semisynthetic approach by incorporating a well-characterized, small molecule catalyst into an existing metalloprotein scaffold. $[Ni^{II}(cyclam)]^{2+}$, (([**1**]), cyclam = 1,4,8,11-tetraazacyclotetradecane) has received a great deal of attention because of reported catalytic selectivity for CO_2 reduction to CO in water. While much of the early work was conducted using a mercury-based electrode, recent literature reports indicate that CO_2 can also be reduced to CO by [**1**] using a glassy carbon electrode under aqueous conditions.[18–21] Since those initial studies, a variety of approaches have been explored to improve the catalytic properties of [**1**], including attachment to a conducting polymer,[22] semiconductor,[23,24] and ruthenium phototrigger.[25] Variations on the ruthenium photosensitizer used have also been reported.[26] In our own lab, incorporation of [**1**] into distinct sites within the azurin (Az) protein scaffold was used to yield active constructs with decreased catalytic overpotentials, higher turnover numbers, and increased selectivity for CO_2 reduction.[17] To further develop this system towards solar fuel applications, a ruthenium-based chromophore has been covalently attached to azurin in a site-selective fashion (RuAz). A single, surface-accessible histidine residue at position 83 was then used

to incorporate $[Ni^{II}(cyclam)]^{2+}$ into the protein via axial coordination of [**1**] to histidine.[17,22] The resultant ternary RuMAz-[**1**] constructs are highly selective catalysts for CO_2 reduction to CO. Gas chromatography (GC), luminescence, time-correlated single photon counting (TCSPC), and Stern-Volmer (SV) quenching experiments were performed on all RuMAz-[**1**] systems to characterize catalytic activity. Ultimately, study of these and related semisynthetic enzymes can provide insight into the catalytic mechanism of CO_2 reduction by [**1**] and reveal key molecular interactions controlling catalyst selectivity.

It was previously shown that coordination of [**1**] to the native His83 residue in Az resulted in the greatest selectivity increase for CO production over H_2 evolution relative to free [**1**] when measured via solution-phase, light-driven assays.[17] Following from this observation, scaffolds containing this native histidine were further developed. Three Az variants were engineered (S66C, S78C, and S100C), each containing a single, surface-exposed cysteine residue located ~11, 12, and 19 Å from His83, respectively (Figure 1A, Figure S1). Using methodology developed by the Cheruzel group, in which metal-based polypyridyl compounds bearing an epoxide functional group can be selectively and quantitatively attached to the sulfhydryl moiety of a cysteine residue,[27] a ruthenium(II) phototrigger (Figure 1B, $[Ru(bpy)_2(epoxy\text{-}phen)]^{2+}$ = [Ru(2,2'-bipyridine)$_2$(5,6-epoxy-5,6-dihydro-[1,10] phenanthroline)]$^{2+}$) was covalently coupled to Az, generating a series of ruthenium-labelled constructs (RuAz) (Figure S2). The resultant RuMAz proteins were then incubated with [**1**] to generate ternary RuMAz-[**1**] complexes. Desalting columns were used immediately prior to running all of the protein-based experiments in order to remove excess [**1**] from solution. To verify the incorporation of [**1**] into each scaffold, cyclic voltammetry was performed, monitoring the position and intensity of the $Ni^{III/II}$ couple of [**1**] at approximately +700 mV vs. NHE (Figures S3-S5, Table S1). The integrated area of this transition relative to the area of the $Cu^{II/I}$ couple was used to estimate the efficiency of [**1**] incorporation into the protein, which was found to be approximately 40%, consistent with our prior report (Figure S5).[17] Because Az also has an endogenous metal binding site that typically contains copper but can be substituted with other divalent metals,[11] both the Cu- and Zn-bound derivatives (RuCuAz, RuZnAz) were studied to probe the effects of including a redox-active metal center within the scaffold.

Enzyme activity was characterized with a light-driven assay coupled to gas chromatography (GC) analysis, using ascorbate as a sacrificial electron donor.[16] Following irradiation with 447 nm light, all RuMAz-[**1**] constructs were shown to catalytically reduce CO_2 to CO (Figure 2). Catalysis was only observed when all reaction components were included. Control assays lacking ascorbate, light, [**1**], or CO_2, including assays with RuMAz in the absence of [**1**], did not produce any detectable amounts of CO (< 50 pmol) over the 2-hour irradiation period. This suggests that the CO produced is exclusively due to reduction of the added CO_2 by [**1**] and cannot be attributed to other carbon sources in the reaction mixture. It is noted that after approximately two and a half hours, trace amounts of CO began to appear in the control experiments, which may be attributed to degradation of the Ru phototrigger and/or Az protein (Figure S6, Table S2). To eliminate any possible contribution of background CO signals, all assays were restricted to two hours.

The most active variant was S78C-RuCuAz-[**1**], which converted 23 +/− 1 nmoles of CO_2 to CO over the two-hour irradiation period; this corresponds to a turnover number (TON) of 4.6 ± 0.2 when the ~40% labelling efficiency of [**1**] to Az is considered.[17] A moderate dependence of activity on distance between the Ru chromophore and [**1**] is observed, as the 78 position is closest to the His83 attachment site. Correspondingly, the S100C-RuAz-[**1**] variants, which place the Ru compound and His83 at the greatest separation distance, exhibit the lowest levels of activity. Interestingly, while our prior study found the Cu-substituted scaffolds to be substantially more active than their Zn-substituted counterparts, metal identity in the native Az binding site does not affect activity of RuMAz-[**1**]. This suggests that intramolecular electron transfer (ET) from the Ru center dominates over ET from Cu, a feasible hypothesis considering the relative reduction potentials (Figure S7).[17]

The protein-based constructs were slightly less active for CO production than control assays containing [**1**] and stoichiometric amounts of $[Ru(bpy)_3]^{2+}$, with absolute quantum yields for CO production by the enzymes ranging from 6.9×10^{-5} to 1.4×10^{-4} (Table S3).[28] However, during the entire irradiation period, the control experiments with free [**1**] displayed poor product selectivity, with a selectivity ratio ($SR = TON_{CO}/TON_{H2}$) of ~0.1 (Figure S8). This low degree of selectivity is consistent with previous reports on light-driven, solution-phase catalysis for CO_2 reduction by [**1**] in aqueous solutions,[17,28–30] though short bulk electrolysis experiments on [**1**] show greater relative efficiencies for CO_2 reduction.[19] In contrast, all ternary RuMAz-[**1**] complexes exclusively produce carbon monoxide, with *no measurable amounts of hydrogen detected* even after two hours of irradiation! While prior studies demonstrated that increased SRs can be obtained by synthetically linking [**1**] to $[Ru(bpy)_3]^{2+}$, co-immobilising [**1**] with a photosensitizer on an inert support system, directly attaching [**1**] to ZnSe quantum dots, and installing [**1**] within Az,[17,29,31,32] these results on RuAz-[**1**] indicate that both an intramolecular electron transfer pathway and a carefully constructed outer coordination sphere are required to generate a catalyst that is completely selective for CO_2 reduction to CO in water. This remarkable observation highlights the complex interplay of factors contributing to catalytic selectivity. Moreover, the activity of these constructs can be related to the behaviour of native Ni-containing carbon monoxide dehydrogenase enzymes, which are highly selective for CO_2 over H^+ reduction and feature a chain of iron-sulfur clusters to promote rapid ET as well as a conserved secondary coordination sphere around the active site.[33]

To further characterize the RuMAz-[**1**] systems, steady-state and time-resolved luminescence studies were carried out on the ternary constructs and corresponding RuMAz controls. The presence of Cu in the Az active site quenches the Ru emission intensity slightly (Figure S9), either via energy transfer or rapid excited-state ET.[34,35] The addition of [**1**] to His83 in RuMAz perturbs not only the emission intensity but also the emission energy. A hypsochromic shift in the peak luminescence wavelength is observed for all constructs (Figures 3A, S10-S11, and Table S4). The most pronounced change, from λ_{max} = 614 nm to λ_{max} = 608 nm, is observed for S78C-RuAz-[**1**] in both the Zn- and Cu-bound systems, which likely stems from the close proximity between [**1**] and the Ru chromophore. Model studies on $[Ru(bpy)_3]^{2+}$ indicate higher dielectric constants are correlated with lower energy transitions;[36] thus, the shifts to higher energy upon addition of [**1**] likely reflect an overall

decrease in local polarity for the ternary constructs. The molecular basis for this change remains under active investigation but may be associated with charge levelling of Az upon addition of a divalent cation or increased local shielding.[37] Along with the shift to higher energies, emission intensities are also slightly greater for the RuMAz-[**1**] systems than RuMAz under non-catalytic conditions (Figure S12).

Time-correlated single-photon counting experiments were used to probe the photophysics of these systems. Simple exponential functions were used to fit the data: a monoexponential function was used for $[ru(bpy)_3]^{2+}$; the ruznaz samples required two components, with increased dynamics as previously seen for attachment of a phototrigger to a protein,[38] and triple exponential decay functions were used to fit the rucuaz traces (figures 3b, s13-s16, and tables s5-s6). the addition of [**1**] did not affect the number of components required to accurately fit the data, so additional elements were not added. unexpectedly, but consistent with the higher emission energies and intensities, increased lifetimes were observed upon the addition of [**1**] to the rumaz scaffold in all cases (figure 3b). this correlation would be anticipated on the basis of the energy gap law, which predicts decreased non-radiative rates for higher energy transitions on the basis of decreased overlap (figure s17) and suggests the dominant effects of [**1**] on the photophysical properties of the ru phototrigger are only these slight shifts in emission energies. these differences likely emerge due to electrostatic interactions.[39,40] the increased average lifetimes exclude the possibility of direct et between the excited $*ru^{ii}$ center and [**1**], rendering this an unlikely step for catalysis. instead, the ru^{i} species generated through quenching of the $*ru^{ii}$ excited state by ascorbate is suggested to be the catalytically relevant reductant. subsequent intramolecular et from ru^{i} to the ni^{ii} center of [**1**] initiates co_2 binding and conversion. it is this intramolecular step that is sensitive to the separation distance between ru^{i} and [**1**], giving rise to the distance dependence seen in the photochemical assays. the proposed pathway for photodriven catalysis based on these observations is illustrated through a modified latimer diagram (figure 4).

In addition to demonstrating the highest levels of catalytic activity, the s78c-rumaz-[**1**] constructs showed the greatest changes in luminescence wavelength and emission lifetimes upon addition of [**1**]. as such, this variant was selected for study to better understand productive and non-productive interactions under catalytic conditions. quenching experiments were performed using four different reducing agents, including ascorbate (asc), dithionite (dt), diethyldithiocarbamate (dtc), and 4-methoxy-N, N-dimethylaniline (*p*-MeODMA).[41–43] While all have sufficient driving force to reduce $*Ru^{II}$ to Ru^{I} and the first three are irreversible electron donors, only Asc is effective for driving catalytic reduction of CO_2 to CO by either [**1**] + $[Ru(bpy)_3]^{2+}$ or S78C-RuZnAz-[**1**] in the light-driven assays (Figure S18).[44,45] To begin to elucidate the mechanism behind this unpredicted behaviour, Stern-Volmer analyses were performed to compare quenching of the S78C-RuZnAz-[**1**] construct relative to S78C-RuZnAz (Figures S19-S22). Decreasing lifetimes and emission intensities were observed, as expected, with increasing concentrations of all quenchers, consistent with a dynamic quenching mechanism. The Stern-Volmer bimolecular rate constants (k_q, M^{-1} s^{-1}) for quenching of $*Ru^{II}$ by each reducing agent were determined from the weighted lifetimes (Table 1).[46–49] The three unproductive reducing agents show essentially diffusion-limited quenching,[46] while the Asc quenching constant is an order of

magnitude slower. Additionally, Asc was the only electron donor for which significant differences in quenching rate occurred upon incorporation of [**1**] into the protein scaffold, as the bimolecular quenching constant increased by approximately 40%. While the origin of this change may be simply electrostatic, identifying distinctions between quenching mechanisms may underlie the differences in reactivity across the set of sacrificial electron donors. For example, measuring the change in quenching constant upon incorporation of [**1**] may serve as a valuable predictor of activity with a given reducing agent.

In conclusion, direct attachment of a ruthenium chromophore to a semisynthetic enzyme generates RuMAz-[**1**] constructs that display complete selectivity for light-driven CO_2 fixation to CO under aqueous conditions. Time-resolved luminescence experiments are dominated by energy gap law effects, indicating direct ET from $*Ru^{II}$ to the nickel center is unlikely, while Stern-Volmer analyses support the observation that productive quenching of the RuMAz-[**1**] constructs occurs only with ascorbate. Ongoing work in our lab aims to directly measure the electron transfer processes between the ruthenium center and [**1**] using transient absorption spectroscopy in order to identify the rate-limiting steps for activity, as well as develop robust catalysts through covalent attachment methods.[50] Ultimately, this work establishes a foundation for development of highly active *and* highly selective catalysts for CO_2 reduction that operate fully in water.

Supplementary Material

Refer to Web version on PubMed Central for supplementary material.

Acknowledgments

We would like to acknowledge Dr. Lionel Cheruzel for helpful advice. This work was supported by the Department of Energy Office of Science with an Early Career Award to H.S.S. (DE-SC0018020). C.R.S. thanks past support by an NIH Chemistry-Biology Interface Training Program Fellowship (GM08512).

References

1. Appel AM, et al. Chem Rev. 2013; 113:6621–6658. [PubMed: 23767781]
2. Bell, AT., et al. Basic research needs: catalysis for energy. Pacific Northwest National Laboratory (PNNL); Richland, WA (US): 2008.
3. Arakawa H, et al. Chem Rev. 2001; 101:953–996. [PubMed: 11709862]
4. Aresta, M., et al. Reaction Mechanisms in Carbon Dioxide Conversion. Springer; Berlin, Heidelberg: 2016. p. 311-345.
5. Costentin C, et al. Proc Natl Acad Sci. 2015; 112:6882–6886. [PubMed: 26038542]
6. Reuillard B, et al. J Am Chem Soc. 2017; 139:14425–14435. [PubMed: 28885841]
7. Sampson MD, et al. J Am Chem Soc. 2014; 136:5460–5471. [PubMed: 24641545]
8. Morris AJ, et al. Acc Chem Res. 2009; 42:1983–1994. [PubMed: 19928829]
9. Mondal B, et al. Curr Opin Chem Biol. 2015; 25:103–109. [PubMed: 25588961]
10. Slater JW, Shafaat HS. J Phys Chem Lett. 2015; 6:3731–3736. [PubMed: 26722748]
11. Manesis AC, Shafaat HS. Inorg Chem. 2015; 54:7959–7967. [PubMed: 26234790]
12. Yu Y, et al. ACS Catal. 2018:1851–1863.
13. Hu C, et al. Chem Commun. 2017; 53:4173–4186.
14. Lewis JC. Curr Opin Chem Biol. 2015; 25:27–35. [PubMed: 25545848]
15. Yu F, et al. Chem Rev. 2014; 114:3495–3578. [PubMed: 24661096]

16. Sommer DJ, et al. Chem Commun. 2014; 50:15852–15855.
17. Schneider CR, Shafaat HS. Chem Commun. 2016; 52:9889–9892.
18. Froehlich JD, Kubiak CP. J Am Chem Soc. 2015; 137:3565–3573. [PubMed: 25714353]
19. Froehlich JD, Kubiak CP. Inorg Chem. 2012; 51:3932–3934. [PubMed: 22435533]
20. Beley M, et al. J Am Chem Soc. 1986; 108:7461–7467. [PubMed: 22283241]
21. Fujihira M, et al. J Electroanal Chem Interfacial Electrochem. 1990; 292:199–215.
22. Saravanakumar D, et al. ChemSusChem. 2012; 5:634–636. [PubMed: 22411895]
23. Neri G, et al. Phys Chem Chem Phys. 2015; 17:1562–1566. [PubMed: 25460350]
24. Wadsworth BL, et al. ACS Catal. 2016; 6:8048–8057.
25. Herrero C, et al. Phys Chem Chem Phys. 2014; 16:12067. [PubMed: 24600692]
26. Montanaro S, et al. Green Process Synth. 2013; 2:335–343.
27. Dwaraknath S, et al. J Inorg Biochem. 2014; 136:154–160. [PubMed: 24468675]
28. Craig CA, et al. J Phys Chem. 1990; 94:7957–7960.
29. Kimura E, et al. Inorg Chem. 1994; 33:770–778.
30. Grant JL, et al. J Chem Soc Dalton Trans. 1987:2105–2109.
31. Neri G, et al. Chem Commun. 2016; 52:14200–14203.
32. Kuehnel MF, et al. Chem Sci. 2018; 9:2501–2509.
33. Can M, et al. Chem Rev. 2014; 114:4149–4174. [PubMed: 24521136]
34. Kostic NM, et al. J Am Chem Soc. 1983; 105:7765–7767.
35. Margalit R, et al. Proc Natl Acad Sci. 1984; 81:6554–6558. [PubMed: 6593716]
36. Caspar JV, Meyer TJ. J Am Chem Soc. 1983; 105:5583–5590.
37. Campagna, S., et al. Photochemistry and Photophysics of Coordination Compounds I. Balzani, V., Campagna, S., editors. Springer; Berlin Heidelberg: 2007. p. 117-214.
38. Ener ME, et al. Proc Natl Acad Sci. 2010; 107:18783–18786. [PubMed: 20947800]
39. Balzani V, et al. Coord Chem Rev. 1998; 171:3–16.
40. Juris A, et al. Helv Chim Acta. 1981; 64:2175–2182.
41. Tran NH, et al. J Am Chem Soc. 2013; 135:14484–14487. [PubMed: 24040992]
42. Mines GA, et al. J Am Chem Soc. 1996; 118:1961–1965.
43. Warren JJ, et al. Chem Rev. 2010; 110:6961–7001. [PubMed: 20925411]
44. Ghosh S, et al. Anal Bioanal Chem. 2010; 397:1573–1582. [PubMed: 20393844]
45. Hall RD, Chignell CF. Photochem Photobiol. 1987; 45:459–464. [PubMed: 3575442]
46. Atik SS, et al. J Am Chem Soc. 1979; 101:5696–5702.
47. Mukherjee TK, et al. Chem Phys Lett. 2005; 407:119–123.
48. Cranney M, et al. Biochim Biophys Acta BBA - Biomembr. 1983; 735:418–425.
49. Fan C, et al. J Am Chem Soc. 2002; 124:5642–5643. [PubMed: 12010029]
50. Zhanaidarova A, et al. Chem Commun. 2018; doi: 10.1039/C8CC00718G

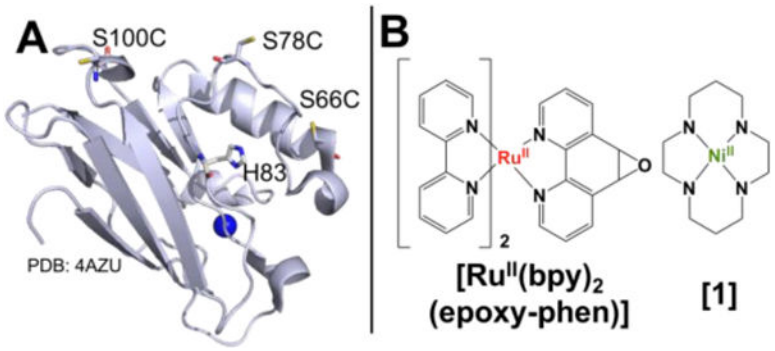

Figure 1.

(**A**) Azurin structure with labelling sites indicated and modeled as Cys residues. (**B**) Structures of small molecules in RuMAz-[**1**] enzymes.

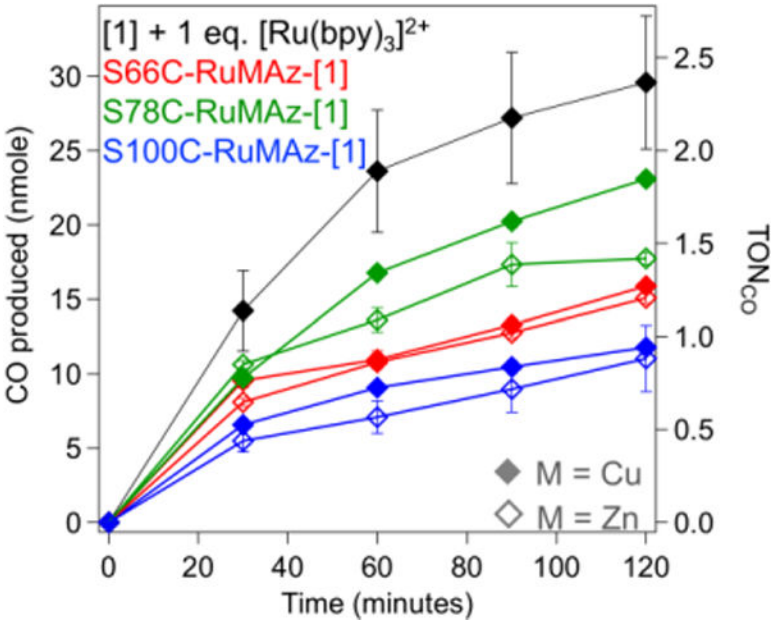

Figure 2.

GC analysis of photoactivity assays (λ_{ex} = 447 nm) containing 5 μM RuMAz-[**1**] or free [**1**] control in 750 mM phosphate/12.5 mM CHES buffer, pH 7.25, with 100 mM ascorbate under a CO_2 atmosphere. TON_{CO} determined with respect to ruthenium concentration.

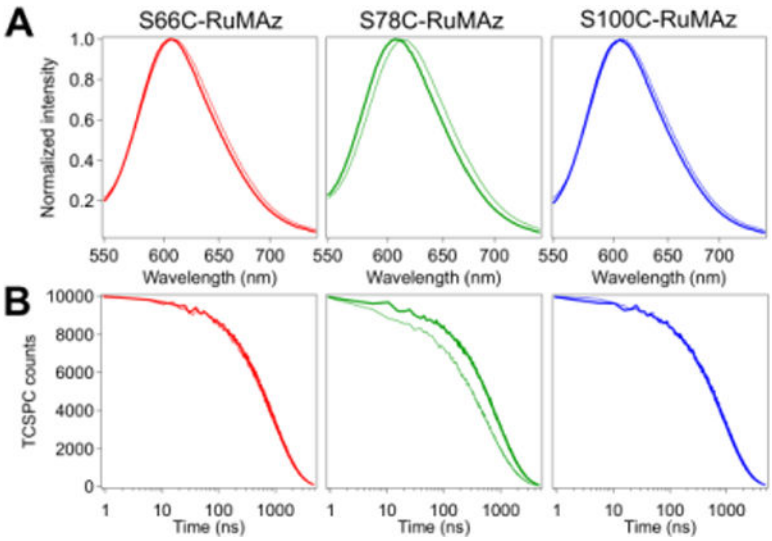

Figure 3.

(**A**) Normalized emission spectra and (**B**) TCSPC decay traces of RuZnAz (thin lines) and RuZnAz-[**1**] (thick lines) as labeled on figure. Samples contain 5 μM protein in 750 mM phosphate/12.5 mM CHES buffer, pH 7.25, under a CO_2 atmosphere.

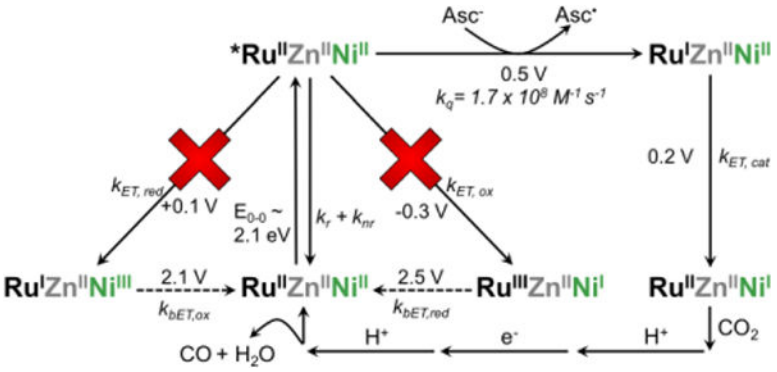

Figure 4.

Modified Latimer diagram illustrating the catalytically relevant pathway for RuZnAz-[**1**]. Reduction potentials and transition energy of the Ru phototrigger and [**1**] taken from prior reports.[17,40]

Table 1

Stern-Volmer bimolecular rate constants (k_q (M^{-1} s^{-1})) for quenching of S78C-RuZnAz and S78C-RuZnAz-[**1**] emission by the indicated reducing agents.

Quencher	S78C-RuZnAz k_q (M^{-1} s^{-1})	S78C-RuZnAz-[1] k_q (M^{-1} s^{-1})
Asc	$1.1 \pm 0.3 \times 10^8$	$1.7 \pm 0.2 \times 10^8$
DT	$1.3 \pm 0.3 \times 10^9$	$1.1 \pm 0.1 \times 10^9$
DTC	$1.3 \pm 0.3 \times 10^9$	$1.5 \pm 0.4 \times 10^9$
p-MeODMA	$9.9 \pm 0.3 \times 10^8$	$9.7 \pm 0.3 \times 10^8$